Physics – Uspekhi **58** (10) 963 – 967 (2015)

PHYSICS OF OUR DAYS

PACS numbers: 13.75.Cs, 13.85.Lg, 14.20.Dh

Universality of hadron cross sections at ultrahigh energies

V V Anisovich

DOI: 10.3367/UFNe.0185.201510c.1043

Contents

Abstract. The current status of ultrahigh energy diffractive collisions is presented. The Gribov total cross section universality is discussed in terms of the profile and *K*-matrix functions in impact parameter space.

Keywords: hadron cross sections, ultrahigh energies, parton disks

1. Introduction

More than 40 years ago, in 1973, Gribov predicted in paper [1] the universality of all hadron cross sections:

$$\sigma_{\rm tot}({\rm pp}):\sigma_{\rm tot}(\pi{\rm p}):\sigma_{\rm tot}(\pi\pi)=1:1:1 \text{ when } \sqrt{s}\to\infty\,. \quad (1)$$

In those days, the data at energies of 50–500 GeV [2–4] pointed to another result (the Levin–Frankfurt relationship [5]):

$$\sigma_{\rm tot}({\rm pp}):\sigma_{\rm tot}(\pi{\rm p}):\sigma_{\rm tot}(\pi\pi)\simeq 9:6:4\,.$$

The situation changed later, when ISR (Intersecting Storage Rings) data [6–10] became available and unambiguously revealed that the total cross sections $\sigma_{\rm tot}$ increase with the collision energy $\sqrt{s}$. This implied the existence of gluon (or glueball) parton clouds as the sources of enhancement of the total cross sections. Modern data obtained at the Large Hadron Collider (LHC) [11–14] and cosmic ray data [15] are consistent with such a picture. At moderately high energies, valence quarks, which are the original source of the formation of parton clouds, provide total cross sections proportional to the number of colliding quarks [5]. As the energy increases, the parton densities also increase, as do the dimensions of the clouds. At LHC energies, the parton clouds start to overlap, which leads to the appearance of a black spot in the profile function (Fig. 1). As a result, not only must the total cross sections undergo changes, but the rearrangement of parton clouds due to an increase in energy must also lead to a change in particle production cross sections; such transformations of spectra in the region of fragmentation production are discussed in Refs [16, 17].

The appearance of a black spot in the profile function at LHC energies has been discussed and commented on in a great number of papers devoted to the increase in total cross sections at ultrahigh energies (see Refs [18–24] and references cited therein). The black disk mode corresponds to incoherent interaction among the partons of colliding hadrons.

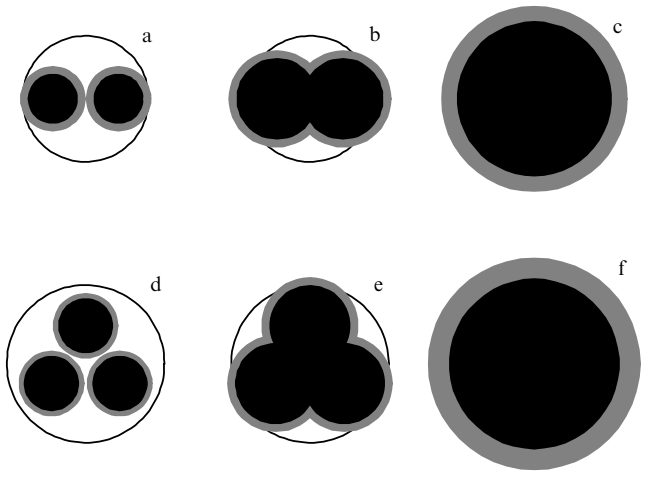

Figure 1. Form of profile functions in impact parameter space for mesons and protons and their transformations with an increase in energy. (a, d) Parton clouds at moderately high energies — the picture is consistent with the Levin–Frankfurt additive model [5]. (b, e) The parton cloud picture at LHC energies, when partial overlapping of clouds takes place and a 'black spot' appears. (c, f) The picture in the region of cosmic ray energies — universal black disks have formed.

V V Anisovich National Research Centre 'Kurchatov Institute' Konstantinov Petersburg Nuclear Physics Institute, Orlova roshcha, 188300 Gatchina, Leningrad region, Russian Federation
E-mail: anisovic@thd.pnpi.spb.ru

Received 4 May 2015, revised 12 June 2015
Uspekhi Fizicheskikh Nauk **185** (10) 1043 – 1047 (2015)
DOI: 10.3367/UFNr.0185.201510c.1043
Translated by G Pontecorvo; edited by A Radzig

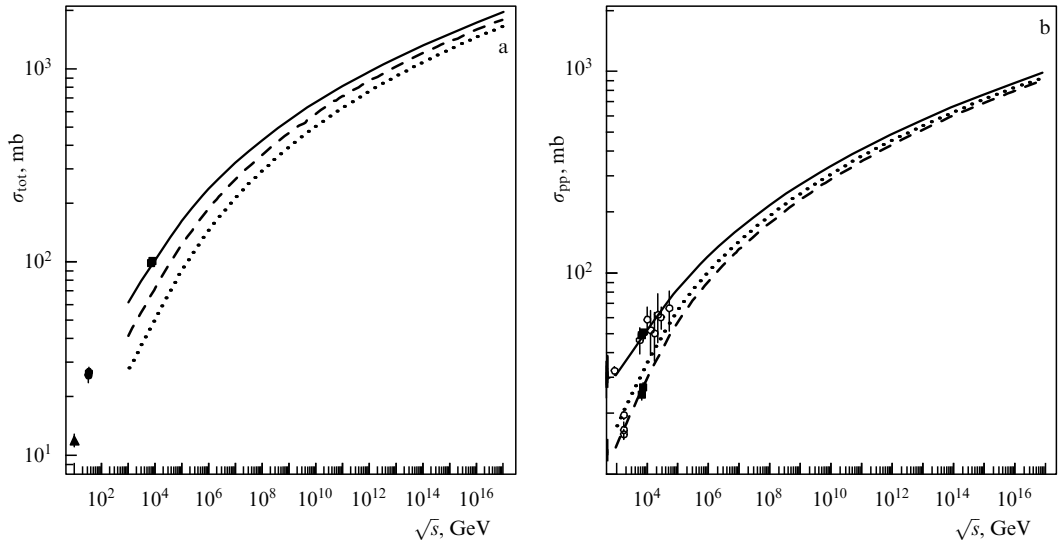

Figure 2. (a) Total cross sections $\sigma_{tot}(pp)$ (solid curve), $\sigma_{tot}(\pi p)$ (dashed curve), and $\sigma_{tot}(\pi\pi)$ (dotted curve) in the black disk mode. Experimental data: squares (pp)—[11], circles (πp)—[27], triangles ($\pi\pi$)—[28]. (b) Proton–proton collisions: $(1/2)\,\sigma_{tot}(pp)$ (solid curve), $\sigma_{el}(pp) + 2\sigma_{D(p)}(pp)$ (dotted curve), and $\sigma_{el}(pp)$ (dashed curve). In the case of $(1/2)\,\sigma_{tot}(pp)$ and $\sigma_{el}(pp)$, the circles represent experimental data [6–11, 15]; the calculated curves are taken from Refs [22, 23].

2. Asymptotic black disk mode

If the asymptotic mode is realized as the black disk mode, then the behavior of hadron cross sections at ultrahigh energies is predicted by their behavior in the pre-asymptotic region and by restrictions imposed by amplitude unitarity and analyticity conditions. Such a model was proposed by Dakhno and Nikonov [25]. The Dakhno–Nikonov model takes into consideration the quark structure of hadrons, the gluon nature of t-channel interactions, and color screening effects in collisions. The model may be considered as an extension of the Good–Walker eikonal approximation [26] to a continual number of channels. Application of the model [25] to the region of asymptotic energies has been performed in Refs [22, 23].

The growth of total cross sections in the black disk mode is illustrated in Fig. 2a for $\sigma_{tot}(pp)$, $\sigma_{tot}(\pi p)$, and $\sigma_{tot}(\pi\pi)$. Relationship (1) is seen to be fulfilled with a 15% accuracy at $\sqrt{s} \sim 10^{15}$ GeV. For comparison, Fig. 2b presents proton–proton characteristics that in the black disk mode case are related as follows:

$$\frac{1}{2}\,\sigma_{tot}(pp) : \sigma_{el}(pp) : \sigma_{el}(pp) + 2\sigma_{D(p)}(pp) = 1:1:1\,;$$

such a relationship is fulfilled with a 15% accuracy at significantly lower energies, $\sqrt{s} \sim 10^7$ GeV. This means that the behavior of total cross sections becomes universal at energies at which the lateral dimensions of parton clouds are significantly greater than the dimensions of static hadrons.

The asymptotic growth of the parton disk is determined by parameters of the leading t-channel singularity: the pomeron intercept, $\alpha(0) = 1 + \Delta$, where $\Delta \simeq 0.25-0.300$, and the slope of the pomeron trajectory α'_P. The leading pomeron is formed by the effective gluons (G), which have a large mass $m_G \sim 700-1000$ MeV [29, 30]. The slope parameter of the pomeron trajectory is small, $\alpha'_P \simeq (0.13-0.25)$ GeV$^{-2} \sim 1/(4m_G^2)$, which corresponds to a heavy pomeron (Gribov [31]). These characteristics of the leading pomeron yield a value of $R_{\text{black disk}} \simeq 2\sqrt{\Delta\alpha'_P}\,\ln s$ for the black disk radius, where $2\sqrt{\Delta\alpha'_P} \simeq 0.08$ fm [22, 23].

Unitarization of the scattering amplitude in the s-channel suppresses the strong pomeron singularity, transforming it into a multipomeron one. Thus, we observe here an intersection of the problems of the gluon composition of the t-channel exchange at ultrahigh energies and of the physics of gluon states — glueballs. At present, glueball states are actively being discussed (see, for instance, Refs [32–34] and references cited therein). Studies of glueball states and of states with rich gluon components, such as the σ-meson, are quite informative for investigating the confinement singularity [35, 36]. The large mass of the soft effective gluon and the slow growth of the black disk radius at ultrahigh energies turn out to be mutually related phenomena.

3. Profile function of scattering amplitude in impact parameter space and the *K*-matrix representation

The black disk mode is usually discussed in terms of the profile function and optical density; in considering other asymptotic modes, it happens to be quite convenient to take advantage of the K-matrix representation of the scattering amplitude. At high energies, the profile function in the impact parameter representation, $T(b)$, is expressed as

$$\begin{aligned}
&\sigma_{tot} = 2\int d^2b\, T(b)\,,\\
&A_{el}(\mathbf{q}_\perp^2) = i\int d^2b \exp(i\mathbf{b}\mathbf{q}_\perp)\, T(b)\,,\ 4\pi\,\frac{d\sigma_{el}}{d\mathbf{q}_\perp^2} = \left|A_{el}(\mathbf{q}_\perp^2)\right|^2,\\
&T(b) = 1 - \eta(b)\exp\left(2i\delta(b)\right) = 1 - \exp\left(-\frac{1}{2}\,\chi(b)\right)\\
&\qquad = \frac{-2iK(b)}{1 - iK(b)}\,,
\end{aligned} \tag{2}$$

where $A_{el}(\mathbf{q}_\perp^2)$ is the elastic scattering amplitude. The profile function can be represented either in the standard form,

applying the inelasticity parameter $\eta(b)$ and the phase shift $\delta(b)$, or in terms of the optical density $\chi(b)$ and the K-matrix function $K(b)$. The K-matrix approximation is based on extraction of the elastic rescatterings in the intermediate states of the amplitude; therefore, function $K(b)$ only contains multiparticle states, thus being a complex quantity. The fact that quantity $\mathrm{Re}\,A_{\mathrm{el}}/\mathrm{Im}\,A_{\mathrm{el}}$ is small at high energies tells us that function $K(b)$ is dominantly imaginary.

Figures 3a and 4a plot the profile function $T(b)$ and the K-matrix function $-\mathrm{i}K(b)$ for pp collisions in the black disk mode. In the region of pre-asymptotic energies, $\sqrt{s} \leqslant 1$ TeV, function $-\mathrm{i}K(b)$ increases with energy and is concentrated around $b < 1$ fm. In the case of ultrahigh energies, the black disk mode signifies 'freezing' of the K-matrix function, $-\mathrm{i}K(b) \to 1$, in the disk region.

However, the black disk mode does not bring the total cross sections up to their maximum values; the maximum total cross sections are realized when $-\mathrm{i}K(b) \to \infty$ and $T(b) \to 2$ [37–39].

4. Asymptotic resonant disk mode

If $-\mathrm{i}K(b)$ continues to increase with energy, then the interaction region will transform into a resonant disk. The profile function $T(b)$ and the K-matrix function $-\mathrm{i}K(b)$ for a resonant disk are plotted in Figs 3b, 4b. In this case, we observe an asymptotic growth:

$$\sigma_{\mathrm{tot}}(\mathrm{pp}) \sim \ln^2 s\,, \quad \sigma_{\mathrm{el}}(\mathrm{pp}) \sim \ln^2 s\,, \quad \left[\frac{\sigma_{\mathrm{el}}(\mathrm{pp})}{\sigma_{\mathrm{tot}}(\mathrm{pp})}\right]_{s\to\infty} \to 1$$

(Fig. 5). The resonant disk region is surrounded by a black ring (Fig. 6), which leads to relatively slow growth of the inelastic cross sections: $\sigma_{\mathrm{inel}}(\mathrm{pp}) \sim \ln s$, $\sigma_{\mathrm{D}}(\mathrm{pp}) \sim \ln s$, $\sigma_{\mathrm{DD}}(\mathrm{pp}) \sim \ln s$.

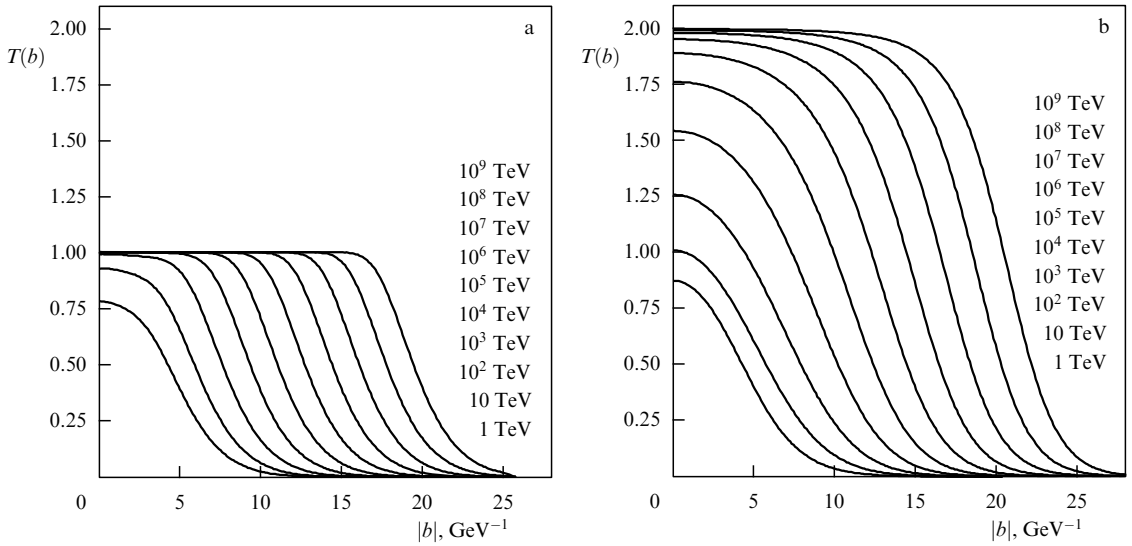

Figure 3. Profile functions $T(b)$ at $\sqrt{s} = 1,\ 10,\ 10^2, \ldots, 10^9$ TeV for (a) the black disk mode: $T(b) \to 1$ [23], and (b) the resonant disk mode: $T(b) \to 2$ [39]. The profile functions in both modes are approximately equal to each other at $\sqrt{s} = 1-10$ TeV.

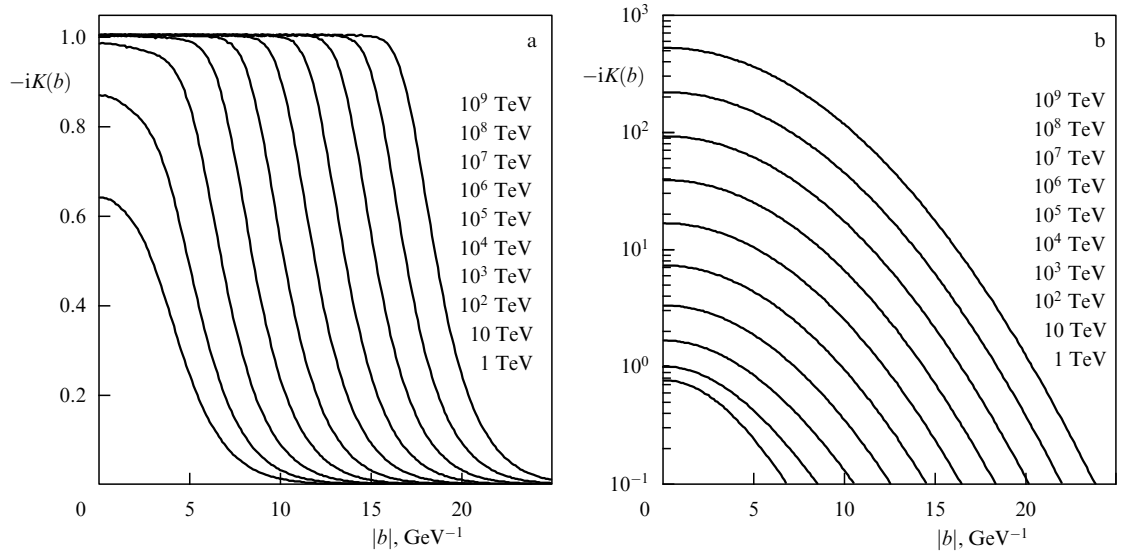

Figure 4. K-matrix function $-\mathrm{i}K(b)$ calculated at energies $\sqrt{s} = 1-10^9$ TeV for (a) black disk mode ($[-\mathrm{i}K(b)]_{\ln s\to\infty} \to 1$ for $b < R_0 \ln s$), and (b) resonant disk mode ($[-\mathrm{i}K(b)]_{\ln s\to\infty} \to \infty$ for $b < R_0 \ln s$). (Taken from Ref. [39].)

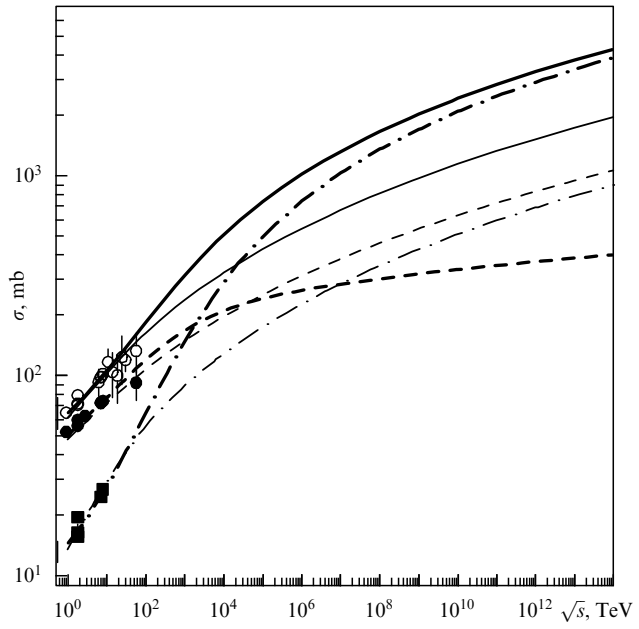

Figure 5. Total, elastic, and inelastic cross sections in the resonant disk mode (bold curves) and in the black disk mode (thin curves): the empty circles and solid curves refer to $\sigma_{\rm tot}$, the squares and dashed–dotted curves to $\sigma_{\rm el}$, and the full circles and dashed curves to $\sigma_{\rm inel}$.

It is clearly seen that a description of experimental data at $\sqrt{s} \sim 1-10$ TeV (see Fig. 5) is not sensitive to the choice of disk version, the initial stages in the growth of cross sections being quite similar in both modes. The differences are noticeable at $\sqrt{s} \sim 10^3-10^4$ TeV.

Indeed, at energies of $\sqrt{s} \sim 10$ TeV the black cloud fills up the static hadron region, $b \leqslant 1$ fm, and this takes place in both modes (see Figs 3, 4): the profile functions $T(b)$ practically coincide, as do $-{\rm i}K(b)$. Respectively, the cross sections $\sigma_{\rm tot}$, $\sigma_{\rm el}$, and $\sigma_{\rm inel}$ also coincide (see Fig. 5).

Differences turn out to be noticeable at $\sqrt{s} \sim 1000$ TeV: in the region of such energies $T(b) \simeq 1.5$ for $b \lesssim 0.5$ fm, while the black zone shifts into the region of $b \simeq 1.0-1.5$ fm (Fig. 3b). With a further increase in energy, the radius of the black belt increases as $2\sqrt{\Delta\alpha'}\,\ln s$. A picture of a parton cloud in the resonant disk mode is displayed in Fig. 6.

The growth rate of cross sections in both modes is determined by leading singularities, and fitting experimental data at $\sqrt{s} \sim 1-10$ TeV yields approximately identical values for Δ and α' in both modes, thus resulting in identical disk radii: $R_{\rm black\ disk} \simeq R_{\rm resonant\ disk}$.

The late onset of the resonant disk mode underlines the importance of experiments with cosmic rays.

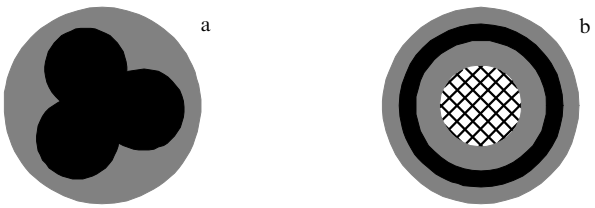

Figure 6. Resonant disk mode; picture of a proton in impact parameter space: (a) the black spot appears at LHC energies, and (b) when the energy increases, the spot transforms into a black belt surrounding the space involving maximum elastic scattering — this is the resonant disk region.

5. Conclusion. Gribov universality of cross sections

The interaction of soft gluons underlies the physics of hadrons. Effective gluons are massive: their mass is on the order of 1 GeV, which follows directly from data on the radiative decays of heavy quarkonia [29, 30], $\psi \to \gamma + {\rm hadrons}$, and $\Upsilon \to \gamma + {\rm hadrons}$. The effective gluon mass is determinative both for low-energy physics (having made it possible to introduce the concept of a constituent quark) and in high-energy physics (having set the rate at which the interaction radius increases). High-energy physics is a physics of large logarithms, $\ln(s/s_0) \gg 1$, and the quantity $\sqrt{s_0} \sim m_{\rm effective\ gluon}$ determines the onset of the asymptotic mode at $\sqrt{s} \sim 1$ TeV. However, characteristics such as $\sigma_{\rm tot}$, $\sigma_{\rm el}$, and $\sigma_{\rm inel}$ measured in the pre-asymptotic region differ weakly, so their behavior at LHC energies does not permit us to identify the mode of the asymptotics. Real differences are seen at $\sqrt{s} \sim 10^3-10^4$ TeV.

Parton disks determine the physics of collisions at ultrahigh energies; the disks are universal for different types of hadrons. Precisely this leads to both total, $\sigma_{\rm tot}$, and diffraction cross sections being universal. Although the mode of the asymptotics has still not been revealed, it can be said with certainty that, whatever the asymptotics, the universality of cross sections holds valid (Gribov [1]).

The data of cosmic ray collisions contain information that may permit the character of the asymptotic mode to be determines. Inelastic diffraction processes differ greatly in different modes [40, 41], and studying them may provide a chance to pave the way towards resolving the problem.

Acknowledgments

The author is grateful to M A Matveev, K V Nikonov, V A Nikonov, and J Nyiri for the useful discussions of the issues dealt with herein. The work was supported by Russian Federation grants RFBR-13-02-00425 and RSGSS-4801.2012.2.

References

1. Gribov V N *Sov. J. Nucl. Phys.* **17** 313 (1973); *Yad. Fiz.* **17** 603 (1973)
2. Denisov S P et al. *Phys. Lett. B* **36** 415 (1971)
3. Carroll A S et al. *Phys. Lett. B* **61** 303 (1976)
4. Carroll A S et al. *Phys. Lett. B* **80** 423 (1979)
5. Levin E M, Frankfurt L L *JETP Lett.* **2** 65 (1965); *Pis'ma Zh. Eksp. Teor. Fiz.* **2** 105 (1965)
6. Arnison G et al. (UA1 Collab.) *Phys. Lett. B* **128** 336 (1982)
7. Bozzo M et al. (UA4 Collab.) *Phys. Lett. B* **147** 385 (1984)
8. Amos N A et al. (E-710 Collab.) *Phys. Lett. B* **247** 127 (1990)
9. Augier C et al. (UA4/2 Collab.) *Phys. Lett. B* **316** 448 (1993)
10. Abe F et al. (CDF Collab.) *Phys. Rev. D* **50** 5518 (1994)
11. Latino G (on behalf of TOTEM Collab.) "Summary of Physics Results from the TOTEM Experiment" *EPJ Web Conf.* **49** 02005 (2013); arXiv:1302.2098
12. Aad G et al. (ATLAS Collab.) *Eur. Phys. J. C* **72** 1926 (2012); arXiv:1201.2808
13. CMS Collab. "Measurement of diffraction dissociation cross sections at $\sqrt{s} = 7$ TeV at the LHC", CMS-PAS-FSQ-12-005 (2013)
14. Abelev B et al. (ALICE Collab.) *Eur. Phys. J. C* **73** 2456 (2013); arXiv:1208.4968
15. Abreu P et al. (The Pierre Auger Collab.) *Phys. Rev. Lett.* **109** 062002 (2012)
16. Anisovich V V, Shekhter V M *Sov. J. Nucl. Phys.* **28** 561 (1978); *Yad. Fiz.* **28** 1079 (1978)
17. Anisovich V V, Levin E M, Ryskin M G *Sov. J. Nucl. Phys.* **29** 674 (1979); *Yad. Fiz.* **29** 1311 (1979)
18. Block M M, Halzen F *Phys. Rev. D* **86** 051504(R) (2012)

19. Uzhinsky V, Galoyan A, arXiv:1111.4984
20. Schegelsky V A, Ryskin M G *Phys. Rev. D* **85** 094024 (2012)
21. Martynov E *Phys. Rev. D* **87** 114018 (2013)
22. Anisovich V V, Nikonov K V, Nikonov V A *Phys. Rev. D* **88** 014039 (2013)
23. Anisovich V V, Nikonov V A, Nyiri J *Phys. Rev. D* **88** 094015 (2013)
24. Dremin I M *Phys. Usp.* **56** 3 (2013); *Usp. Fiz. Nauk* **183** 3 (2013)
25. Dakhno L G, Nikonov V A *Eur. Phys. J. A* **5** 209 (1999)
26. Good M L, Walker W D *Phys. Rev.* **120** 1857 (1960)
27. Dersch U et al. (SELEX Collab.) *Nucl. Phys. B* **579** 277 (2000); hep-ex/9910052
28. Abramowicz H et al. *Nucl. Phys. B* **166** 62 (1980)
29. Parisi G, Petronzio R *Phys. Lett. B* **94** 51 (1980)
30. Consoli M, Field J H *Phys. Rev. D* **49** 1293 (1994)
31. Gribov V N *Nucl. Phys. B* **106** 189 (1976)
32. Anisovich V V *Phys. Usp.* **47** 45 (2004); *Usp. Fiz. Nauk* **174** 49 (2004)
33. Klempt E, Zaitsev A *Phys. Rep.* **454** 1 (2007)
34. Ochs W *J. Phys. G Nucl. Part. Phys.* **40** 043001 (2013)
35. Anisovich V V, Bugg D V, Sarantsev A V *Phys. Rev. D* **58** 111503(R) (1998)
36. Anisovich A V et al. *Phys. Rev. D* **84** 076001 (2011)
37. Troshin S M, Tyurin N E *Int. J. Mod. Phys. A* **29** 1450151 (2014); arXiv:1408.2650
38. Dremin I M *Phys. Usp.* **58** 61 (2015); *Usp. Fiz. Nauk* **185** 65 (2015); arXiv:1406.2153
39. Anisovich V V, Nikonov V A, Nyiri J *Phys. Rev. D* **90** 074005 (2014); arXiv:1408.0692
40. Anisovich V V, Matveev M A, Nikonov V A *Int. J. Mod. Phys. A* **30** 1550054 (2015); arXiv:1407.4588
41. Anisovich V V et al. *Int. J. Mod. Phys. A* **29** 1450176 (2014); arXiv:1408.4543